PCCP

Accepted Manuscript

ROYAL SOCIETY OF CHEMISTRY

www.rsc.org/pccp

PCCP

ARTICLE

Divalent Metal Ion-Mediated Assembly of Spherical Nucleic Acids: The Case Study of Cu^{2+}

Received 00th January 20xx,
Accepted 00th January 20xx

DOI: 10.1039/x0xx00000x

www.rsc.org/

Jang Ho Joo [a] and Jae-Seung Lee*[a]

Despite the critical functions of divalent metal ions (M^{2+}s) in association with duplex DNA, fundamental and general interactions of M^{2+}s with spherical nucleic acids (SNAs) composed of single-stranded DNA have rarely been investigated. We have explored that the coordinative nature of the M^{2+}-SNA binding mediates the temperature- and base composition-dependent reversible assemblies of SNAs even without the need of complementary counterparts for duplex-interconnection, additional monovalent metal ions for charge screening, or pre-designed sequences for any non-Watson-Crick base-pairing, all of which are essential for the conventional assembly of SNAs. Cu^{2+} has been identified to maximize the reversible assembly properties in relation to this M^{2+}-mediated DNA bond, and has been further qualitatively and quantitatively investigated in detail as a model system.

Introduction

The conceptual development of spherical nucleic acids (SNAs)[1, 2] has led to their various advanced applications in areas such as materials synthesis, biochemical diagnostics, and clinical therapeutics.[3-9] Such versatility of SNAs stems from their distinctive chemical and physical assembly properties, including reversibility, programmability, cooperative binding, and sharp melting transitions.[10] In spite of the current diversity of the assembly modes of SNAs, these unique assembly properties, once the structure of the SNA is determined, are fundamentally and precisely controlled by the solution conditions,[11-13] particularly the metal ion concentration. Typically, Na^+ is used at a desired concentration to reduce the negative charge of SNAs and thus stabilize the duplex interconnects of the SNA assemblies. Other monovalent metal ions also induce the assembly of SNAs based on the formation of G-quadruplex, cytosine-cytosine or guanine-guanine mismatches, by additional stabilization.[14-19] In comparison to monovalent ions, divalent metal ions (M^{2+}s) are expected to exhibit a stronger stabilizing effect on DNA duplex formation because of their higher charge. In fact, to achieve a given melting temperature (T_m) of a short linear duplex, M^{2+}s are required only at a concentration two orders of magnitude lower than that required for monovalent metal ions owing to their higher association constants.[20] In addition, the coordination of mercuric ion (Hg^{2+}) to a specific thymine-thymine mismatch of SNA assemblies also stabilizes the duplex interconnects.[21, 22] These results certainly provide insights into the interactions of M^{2+}s with nucleic acids, but they are mainly focused on conventional free duplex DNA strands. To date, the chemical functions of M^{2+}s in controlling the assembly properties of SNAs are not sufficiently understood, and need to be thoroughly examined.

Herein, we present a systematic investigation of the chemical interactions of various M^{2+}s with SNAs. Importantly, we demonstrate that M^{2+}s are inherently capable of inducing the reversible assembly of single-type SNAs via coordination chemistry even without their complementary SNAs. In particular, cupric ion (Cu^{2+}) substantially maximizes these unique assembly properties, and is investigated as a case study. Gold nanoparticles (gold NPs) are used as a core of the SNAs, and their surface plasmon resonance is taken advantage of for easily observing the assembly properties of the SNAs using UV-vis spectroscopy.[23, 24]

Results and discussion

We first prepared conventional duplex-interconnected assemblies of SNAs (**S1** and **S2**, see Experimental) in the presence of NaCl (0.15 M), and began our investigation of how their dissociation properties were affected by M^{2+}s by spiking one of seven M^{2+}s including an alkali earth metal (Mg^{2+}) and period 4 and 5 transition metals (Mn^{2+}, Co^{2+}, Ni^{2+}, Cu^{2+}, Zn^{2+}, Cd^{2+}), and by obtaining their melting transitions (see Figure S1, †ESI). Addition of more Na^+ was also evaluated for comparison. Subsequently, we obtained their melting temperatures (T_ms)[10] as a function of [M^{2+}] from 0 to 2.5 mM (Figure 1a). In the absence of the M^{2+}s or additional Na^+, the eight batches of SNA assemblies exhibited a practically identical T_m of 41.1 °C. As the M^{2+} concentration increased, however, the resulting changes to the T_m were strikingly different depending on the type of M^{2+} added. Most of the M^{2+}s (Mg^{2+}, Mn^{2+}, Co^{2+}, Ni^{2+}, and Zn^{2+}) and Na^+ consistently increased T_m, with various slopes. In contrast, however, Cd^{2+} and Cu^{2+} decreased the T_m as their concentrations increased. To our surprise, Cu^{2+} exhibited a particularly dramatic decrease in T_m even below 0.25 mM (slope = -46 °C/mM), which is an even larger decrease than that exhibited by Cd^{2+} (slope = -1.3 °C/mM). Importantly, to the best of our knowledge, this negative effect of Cu^{2+} and Cd^{2+} on the T_m was observed for the first time with conventional SNA assemblies, and is exactly opposite to what is expected from the DNA charge-screening effect of metal ions. The effect of the M^{2+}s on duplex

[a] Department of Materials Science and Engineering, Korea University, 145 Anam-ro, Seongbuk-gu, Seoul, 02841 Republic of Korea
*E-mail: jslee79@korea.ac.kr

†Electronic Supplementary Information (ESI) available: R^2 of the linear fit, melting transitions of SNA assemblies with M^{2+}, UV-vis spectra of assembled SNAs at various [Cu^{2+}]s, and additional kinetic data.

interconnects of SNAs was further clearly demonstrated by comparing the slopes of the curves for T_m vs. $[M^{2+}]$: $Mg^{2+} > Mn^{2+} > Zn^{2+} = Co^{2+} > Ni^{2+} >$ zero $> Cd^{2+} > Cu^{2+}$ (Figure 1a, inset; see Table S1, †ESI). Noticeably, the

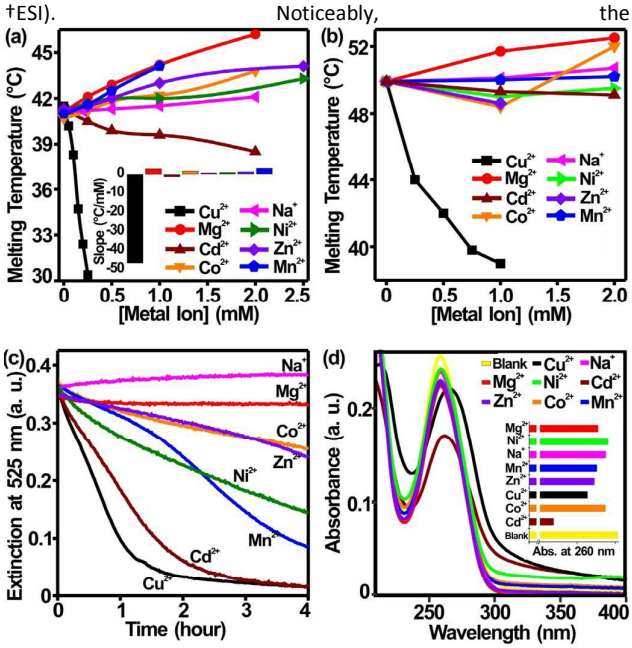

Figure 1. (a) T_ms of duplex-interconnected complementary SNA aggregates (**S1** and **S2**) at various concentrations of M^{2+}s (the initial T_m = 41.1 °C). The slopes were obtained by linear fitting of the curves (inset). (b) T_ms of of short DNA duplexes (**Dbl-S1** and **Dbl-S2**, each at 1 μM, NaCl = 0.15M,) at various concentrations of M^{2+}s (the initial T_m = 49.9 °C). (c) Extinction changes of single-type SNAs (**S1**) in the presence of various M^{2+}s (1 mM) as a function of time. (d) UV-vis spectra of free single-stranded DNA (**FS1**) in the presence of M^{2+}s at 1 mM, and the corresponding absorbance at 260 nm (inset). Note that Cd^{2+} induced the largest decrease in absorbance at 260 nm, followed by Cu^{2+}.

absolute value of the slope of Cu^{2+} was more than 30 times higher than the average of the slopes of the other M^{2+}s, indicative of the substantial and exclusive effect of Cu^{2+} on the binding of the complementary SNAs. In fact, the effect of M^{2+} on T_ms was previously observed with much larger genomic DNA (Type I calf thymus) in a similar manner.[25] In addition, we also obtained a similar trend with short DNA duplexes (**Dbl-S1** and **Dbl-S2,** see Experimental) as demonstrated in Figure 1b, demonstrating the consistency of the hybridized SNA-M^{2+} and free DNA duplex-M^{2+} interactions.

In addition to the duplex-interconnected SNA assemblies, the interactions of dispersed single-type SNAs with M^{2+}s were also kinetically studied. We combined the dispersed single-type SNAs (**S1**) with each M^{2+} (1 mM) and monitored the extinction of the core gold NPs, an optical measure of their assembly status, as a function of time using UV-vis spectroscopy. Unexpectedly, all the M^{2+}s induced the assembly formation of the SNAs without the complementary SNAs, yet exhibited different kinetic rates (Figure 1c). Cu^{2+} induced the most rapid assembly formation of the SNAs, closely followed by Cd^{2+}. This result implies that SNA assembly formation is not based on simple electrostatic charge screening, but relies on an additional 'specific' chemical interaction. The kinetically different assembling abilities of M^{2+}s were determined by obtaining the UV-vis spectra of the core gold NPs at 525 nm after 4 h: $Cu^{2+} > Cd^{2+} > Mn^{2+} > Ni^{2+} > Co^{2+} = Zn^{2+} > Mg^{2+}$ (see Figure S2, †ESI). Interestingly, the orders of the M^{2+}s in Figures 1a and 1c are almost opposite, indicating that the M^{2+}-mediated 'specific' chemical interaction 'disassembles' the DNA duplexes, and 'assembles' the single strands.

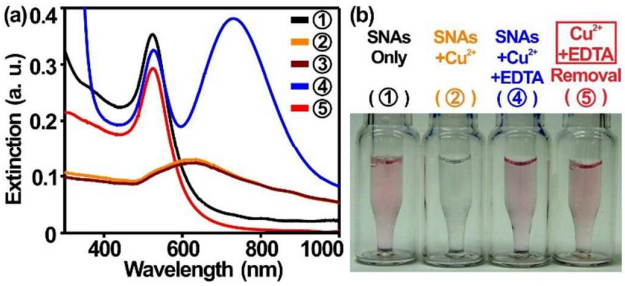

Figure 2. (a) UV-vis spectra of ① dispersed SNAs (**S1**), ② assembled SNAs by Cu^{2+} (1.2 mM), ③ assembled SNAs by Cu^{2+} (1.4 mM), ④ dispersed SNAs by EDTA, and ⑤ dispersed SNAs after the removal of Cu^{2+}-EDTA complex. The spectra of assembled SNAs at more specific $[Cu^{2+}]$s from 0 to 1.4 mM are shown in Figure S3, †ESI. (b) Visual observation of the SNA solutions (①, ②, ④ and ⑤). Note that ④ appear purple in spite of the dispersed SNAs because of the blue color of the Cu^{2+}-EDTA complex. The color of ④ turned red after the removal of Cu^{2+}-EDTA complex (⑤).

The M^{2+}-induced assembly of SNAs was comparatively analyzed by examining free single-stranded DNA, the molecular counterpart of SNAs. Previously, the interactions of much larger genomic DNA duplexes with M^{2+}s were spectroscopically investigated and understood to induce DNA condensation or compaction, with a main emphasis on the decrease of the volume occupied by DNA as macromolecular biopolymer.[26, 27] On the other hand, we examined very short, single-stranded free DNA of the same sequence as **S1** (**FS1**, see Experimental) in the presence of M^{2+}s (1 mM), and observed that the absorbance at 260 nm decreased in all cases, particularly with Cd^{2+} and Cu^{2+} (Figure 1d). This observation generally demonstrates the preferred interactions of Cd^{2+} and Cu^{2+} with free single-stranded DNA, as observed with SNAs (Figures 1a and 1c).

Considering the dramatic and distinctive effects of Cu^{2+} on the SNA assembly properties, we selected Cu^{2+} to further understand how M^{2+}s can control SNAs assembly properties. We prepared a series of SNA solutions containing Cu^{2+} at various concentrations (from 0 to 1.4 mM), allowed them to interact for 12 h for assembly formation, and obtained their UV-vis spectra to analyze their $[Cu^{2+}]$-dependent assembly properties (see Figure S3, †ESI). Three representative spectra at 0, 1.2, and 1.4 mM of Cu^{2+} were selected and shown in Figure 2a. As $[Cu^{2+}]$ increased, the λ_{MAX} (the wavelength at which the maximum extinction took place) was gradually red-shifted from 525 to 630 nm, and extinction at the λ_{MAX} decreased by 70% after 12 h owing to the assembly formation of SNAs into larger aggregates (see Figure S3, †ESI). When $[Cu^{2+}]$ was high enough ($[Cu^{2+}] > 1.2$ mM), the spectral change became almost negligible, indicating that assembly formation reached a plateau (Figure 2a, ② and ③). The assembly formation was also observed with bare eyes, exhibiting clear a color change from red to pale blue (Figure 2b). In contrast, the unmodified, citrate-coated gold NPs in the presence of Cu^{2+} (1 mM) did not exhibit any observable spectral and color changes (see Figure S4, †ESI), indicating that the nucleic

acids, not the gold NPs, were responsible for SNA assembly. Because the assembly properties vary among different types and concentrations of M^{2+}s despite their same charge, we hypothesized that the M^{2+}s bind to the SNAs by non-electrostatic and thus potentially coordinative interactions, and examined the reversibility of the SNA assemblies in association with Cu^{2+}. Assuming that the SNA assemblies would reversibly disassemble when Cu^{2+} that was coordinated to multiple bases and potentially linked multiple SNAs was removed from the reaction system, we sequestered the Cu^{2+} from the SNA assemblies using ethylenediaminetetraacetic acid (EDTA), whose binding constant to Cu^{2+} is extremely high (18.7 as a logarithm).[28] Significantly, after the addition of EDTA to the SNA assemblies, the solution immediately turned intense purple (Figure 2b, ④), indicating the disassembly of the SNAs. The UV-vis spectrum of the mixture was resolved into two major extinction bands at 525 and 730 nm, which corresponded to the dispersed SNAs and the Cu^{2+}-EDTA complex, respectively (Figure 2a, ④). Eventually a single plasmon extinction band at 525 nm corresponding to a deep red color of dispersed SNAs was obtained after the removal of the Cu^{2+}-EDTA complex (Figures 2a and 2b, ⑤). The recovery efficiency based on the extinction at 525 nm was calculated to be ~ 90%, confirming that the Cu^{2+}-SNA coordination is reversible.

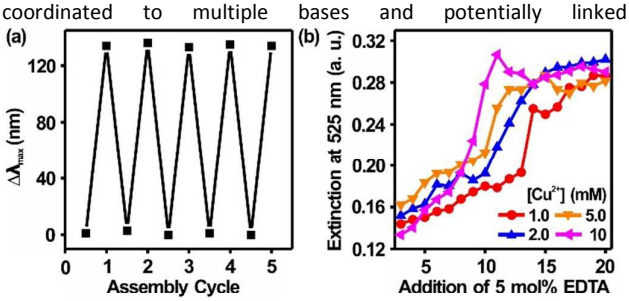

Figure 3. (a) The change in $\Delta\lambda_{MAX}$ by the repeated assembly and disassembly of the SNAs (**S1**). (b) The disassembly profiles of the SNA (**S1**) aggregates as a function of [EDTA] at various initial $[Cu^{2+}]$s.

The reversibility of the Cu^{2+}-mediated SNA assembly was further investigated with respect to the repeatability and cooperativity, unique and distinctive assembly features of conventional duplex-interconnected SNA assemblies. As a measure of the assembly status, the λ_{MAX} of the UV-vis spectrum of the SNAs was observed after the addition and then removal of Cu^{2+}, which was considered to be one assembly cycle (Figure 3a). After the first assembly cycle, repeating the addition and removal of Cu^{2+} (1 mM) to the same batch of the SNAs (1 nM, single-type) induced their assembly and disassembly, respectively, leading to almost the same red-shift (630 nm) and blue shift (525 nm) of the λ_{MAX} as observed in the first cycle. Three more assembly cycles were conducted and yielded similar results, demonstrating the complete reversibility of the Cu^{2+}-mediated SNA assembly.

Based on the confirmed reversibility, we quantitatively analyzed the disassembly properties of the SNAs as a function of the $[Cu^{2+}]$. In brief, we first assembled the single-type SNAs at various concentrations of Cu^{2+} (1, 2, 5, and 10 mM) and observed how they disassembled by monitoring the extinction at 525 nm while the $[Cu^{2+}]$ was gradually decreased by the fractional addition of EDTA aliquots each equivalent to 5 mol% of the initial mole number of Cu^{2+} (Figure 3b). At 1 mM of Cu^{2+}, the extinction of the assembled SNAs at 525 nm almost linearly increased to ~50% of the final extinction as the EDTA aliquots were added up to a final concentration of 65 mol%, indicating the progressive disassembly of the SNAs. Importantly, however, the extinction dramatically jumped to ~85% after one more EDTA aliquot was added (70 mol%), demonstrating cooperative disassembly properties analogous to those of the thermal or $[Na^+]$-dependent disassembly of the conventional duplex-interconnected SNA assemblies.[10, 14] Subsequently, we examined the disassembly properties at a higher initial $[Cu^{2+}]$ (2, 5, and 10 mM) and in general observed cooperative disassembly transitions in a similar way. At all the concentrations of Cu^{2+}, the disassembly profiles of SNAs consisted of three distinctive steps based on their optical properties: (1) gradual disassembly as a function of [EDTA] in a linear manner, (2) dramatic completion of disassembly by a small increase of [EDTA] (~10 mol%), and (3) no further change of stably and individually dispersed SNAs at higher [EDTA]. Interestingly, as the initial $[Cu^{2+}]$ increased, the cooperative disassembly began to take place at a lower mol% of EDTA. This weaker binding of the SNAs at a higher initial $[Cu^{2+}]$ is ascribed to the unbalanced stoichiometry of Cu^{2+} and the bases of the SNAs. At higher initial $[Cu^{2+}]$, more Cu^{2+} than is required to assemble SNAs would not bridge multiple bases, but rather would interact with single bases individually, resulting in more loosely assembled SNAs.

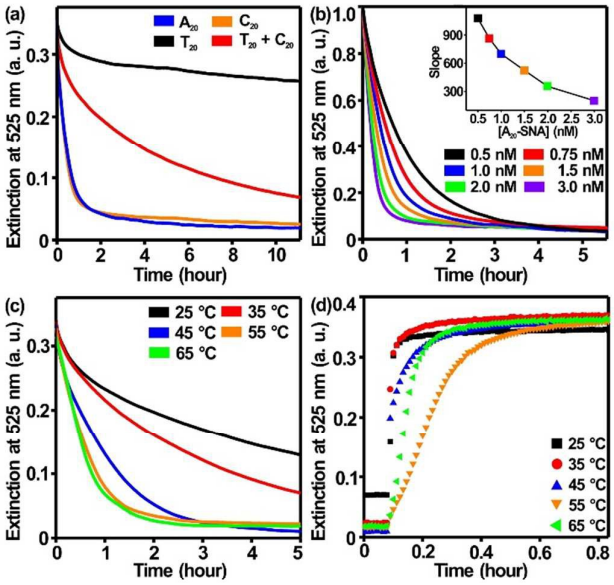

Figure 4. Cu^{2+}-mediated assembly rates of SNAs (a) composed of different bases, (b) at different [SNA]s (**S1**), and (c) at various temperatures (**S1**). (d) EDTA-induced disassembly rates of SNAs (**S1**) at various temperatures.

Based on the reversible assembly properties of SNAs controlled repeatedly and quantitatively by Cu^{2+}, we surmise that the origin of Cu^{2+}'s assembling capability is that Cu^{2+}s are coordinated specifically to nucleobases of SNA (Scheme 1). In fact, previous studies demonstrated that M^{2+}s could bind to the bases of free duplex DNA strands by coordination chemistry.[29-36] In our study, Cu^{2+} and Cd^{2+} strongly coordinated to the electron donor groups of nucleobases in the duplex-interconnected SNA assemblies, and inevitably disturbed the hydrogen bonding between the complementary SNAs significantly enough to decrease the T_m (Figure 1a). In case of the single-type SNAs, most of the M^{2+}s, particularly Cu^{2+}, are possibly able to bind to multiple bases of different individual SNAs to crosslink them into large aggregates

(Figure 1c).[30] We also observed that the SNAs still formed assemblies at a very high [Cu^{2+}] (500 mM) (see Figure S5, †ESI), which implies that the assembly formation could be also partially attributed to the decreased repulsion between SNAs owing to the charge screening by the coordinated Cu^{2+}.[37-39]

In addition to the disassembly properties of the SNAs, the kinetic assembly properties were investigated under various chemical conditions. Although all our observations strongly support the coordinative nature of the interactions between Cu^{2+} and the bases of SNAs, we further conclusively determined the base-dependent

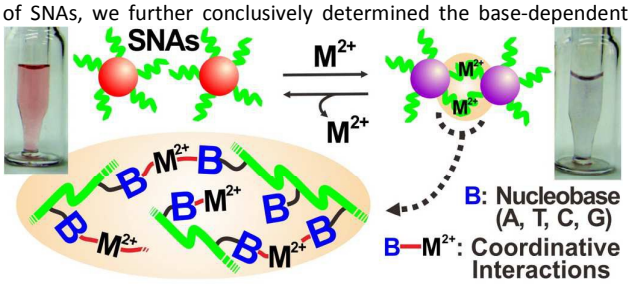

Scheme 1. Schematic illustration of the M^{2+}-mediated reversible assembly of SNAs. Note that the M^{2+}s can coordinate to multiple nucleobases of SNAs, resulting in their cooperative assembly formation with a concomitant color change from red to purple. The assembled SNAs can immediately disassemble once the M^{2+}s are sequestered by stronger ligands, such as EDTA.

kinetic response of the Cu^{2+}-mediated assembly by observing the extinction of SNAs at 525 nm. Because the G-rich SNAs are unstable and easily aggregates owing to G-quadruplex formation in aqueous media,[16] we prepared three types of SNAs, each composed of either polyadenine (**A_{20}**), polycytosine (**C_{20}**), or polythymine (**T_{20}**), and monitored their assembly kinetics in the presence of Cu^{2+} (1 mM, Figure 4a). Importantly, a rapid and significant decrease in extinction was observed for the **A_{20}** and **C_{20}**, both of which reached the minimum observed extinction (~10% of the initial extinction) in less than 2 h. In the case of the **T_{20}**, however, the extinction decreased in a much slower manner, remaining at ~80% of the initial extinction even after 10 h. Importantly, this base-specific binding of Cu^{2+} to the SNAs is in good agreement with the previous infrared spectroscopy and nuclear magnetic resonance studies, where Cu^{2+} was reported to preferentially bind to the N7 position of adenine and N1 of cytosine, but not to bind to any position of thymine owing to its lack of an available nitrogen atom.[40, 41] This specific N7-preference of Cu^{2+} was also theoretically explained in independent studies.[42-44] In comparison, the **T_{20}** and **C_{20}** with Cu^{2+} added at a 1 : 1 molar ratio exhibited an intermediate assembly rate. This remarkable base-dependency apparently indicates that the assembly of the SNAs stems from the coordination of Cu^{2+} to bases of the SNAs, not to phosphates of the backbone. The direction of DNA strands (5′ or 3′ SH) of the SNAs resulted in negligible kinetic differences (see Figure S6, †ESI). In order to examine the effect of the SNA concentration on the assembly kinetics, we observed the change in extinction at various [SNA]s from 0.5 to 3 nM (Figure 4b) at a fixed [Cu^{2+}] (1 mM). As the [SNA] increased, the extinction decreased more steeply, indicating that the SNAs assembled in a faster manner at a higher concentration of the SNAs owing to the increased collision frequency of the SNAs, and thus, the higher chance of their interconnection.[45] The assembly rate curves were linearly fitted in terms of inverse time, and their slopes showed a decreasing trend as the SNA concentration increased (Figure 4b, inset).

We also observed the temperature-dependence of the Cu^{2+}-mediated assembly rate by monitoring the change in extinction of the SNAs (**T_{20}** + **C_{20}** with Cu^{2+} added at 1 : 1) at 525 nm at a range of temperature from 25 to 65 °C. We measured a considerable increase in the assembly rate at higher temperatures (Figure 4c). This observation should be also compared with the duplex-interconnected SNAs, whose assembly rate was previously reported to be rarely affected by the temperature under their T_m.[45] We further investigated the disassembly rates of the SNAs assembled by Cu^{2+} at various temperatures, and observed that, in general, they disassembled more slowly at higher temperatures (Figure 4d). Unlike

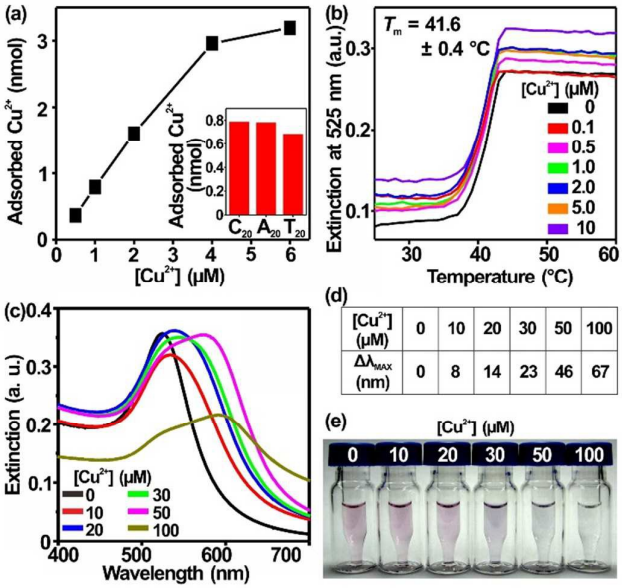

Figure 5. (a) Adsorbed Cu^{2+} to SNAs (**S1**) as a function of the [Cu^{2+}] and type of nucleobases (inset) at low [Cu^{2+}]s ([Cu^{2+}] < 10 μM). (b) Melting transitions of duplex-interconnected SNA assemblies (**S1**, **S2**) in the presence of Cu^{2+} ([Cu^{2+}] < 10 μM). (c) UV-vis spectra of SNAs (**S1**) incubated with Cu^{2+} at physiological [Cu^{2+}]s (10 μM ≤ [Cu^{2+}] ≤ 100 μM). The SNAs and Cu^{2+} were allowed to react at 37 °C for 24 h. (d) The corresponding red-shifts of λ_{MAX} and (e) solution colors of SNAs of Figure 5c.

the conventional duplex-interconnected SNA assemblies, however, the Cu^{2+}-induced SNA assemblies did not reversibly disassemble without EDTA upon heating (see Figure S7, †ESI). Our observations of the assembly and disassembly rates of SNAs as a function of temperature commonly led us to conclude that the Cu^{2+}-mediated assembly formation based on the adsorption of Cu^{2+} to the nucleobases is kinetically favored at higher temperatures. Although the enhanced adsorption of Cu^{2+} to nucleobases of natural genetic DNA at elevated temperatures was previously reported,[46, 47] it was understood only as a result of the increased thermal denaturation of DNA duplexes into single strands, providing more available nucleobases as binding sites for Cu^{2+}. In our result, however, we observed enhanced binding of Cu^{2+} to the single-stranded DNA of the SNAs at higher temperatures, which cannot be explained solely by the mechanism of thermal denaturation. Importantly, to the best of our knowledge, the thermally enhanced rates of Cu^{2+} adsorption to the nucleobases of single-stranded DNA has not been reported to date, and indicates that the kinetic increase in the adsorption reaction needs to be attributed not only to the availability of

nucleobases, but also potentially to the increased binding constant of Cu^{2+} to DNA at a higher temperature.[47]

Despite these results revealing the chemical functions of the M^{2+}s, particularly Cu^{2+}, to control the assembly properties of SNAs, they were demonstrated only at relatively higher [M^{2+}]s around 1 mM (a thousand times as high as [nucleobase] and even a million times as high as [SNA]). To understand the reactions of M^{2+}s at very low concentrations, we combined the SNAs (**S1**, 1 nM) with Cu^{2+} at concentrations almost a thousand times lower than those used in the previous experiments (1 ~ 6 μM, volume = 1 mL), and determined the number of Cu^{2+}s adsorbed to each of the SNAs using inductively coupled plasma mass spectrometry (ICP-MS). Interestingly, the number of adsorbed Cu^{2+}s gradually increased to 3 nmol when [Cu^{2+}] was increased to 4 μM, showing a consistent 75% adsorption of the added Cu^{2+} (Figure 5a). Considering that there was a much smaller number of nucleobases (~1 nmol), this result indicates that the adsorption of Cu^{2+} to SNAs at very low [Cu^{2+}]s involves not only its coordination to nucleobases, but also its electrostatic binding to negatively charged phosphate backbones of the SNAs. To verify this hypothesis, we obtained the numbers of adsorbed Cu^{2+}s at 1 μM to the 3 different types of SNAs (**C_{20}**, **A_{20}**, and **T_{20}**), and observed that **T_{20}** adsorbed almost as many Cu^{2+}s as **A_{20}** and **C_{20}** did (Figure 5a, inset), implying that electrostatic attraction is more dominant between Cu^{2+} and SNAs at low [Cu^{2+}]s. No matter which part of SNA adsorbed Cu^{2+}, however, the assembly properties of duplex-interconnected complementary SNAs were only minimally affected by Cu^{2+} at low [Cu^{2+}]s below 10 μM (Figure 5b). We also investigated the assembly properties of SNAs at concentrations of Cu^{2+} from 10 to 100 μM. This intermediate concentration range is particularly important because it includes the physiological concentration of Cu^{2+} (approximately 20 to 60 μM) in human serum.[48-50] After the incubation of the SNAs with Cu^{2+} at 37 °C, the UV-vis spectra of the SNAs red-shifted in proportion to the [Cu^{2+}] (Figures 5c, 5d and 5e), indicating the [Cu^{2+}]-dependent assembly formation of SNAs. Significantly, this observation demonstrates that SNAs, or potentially any other nanomaterials densely functionalized with DNA, could possibly and unexpectedly assemble into aggregates under physiological conditions simply because of Cu^{2+}, and that DNA-nanomaterial conjugates, including SNAs, should be carefully designed for in vivo applications to minimize such Cu^{2+}-induced assembly formation.

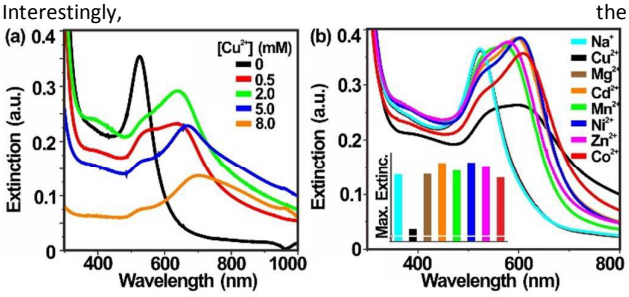

Figure 6. (a) UV-vis spectra of irreversibly assembled SNAs (**S1**) as a function of the [Cu^{2+}] from 0 to 8 mM in the presence of H_2O_2. (b) UV-vis spectra of SNAs whose assemblies were induced by H_2O_2 and each M^{2+} at 0.5 mM. Both Na^+ and Mg^{2+} led to negligible assembly of SNAs, while other transition metal ions induced assembly formation of SNAs to some extent, still with negligible differences in maximum extinction. Only Cu^{2+} resulted in the most significant decrease in maximum extinction. The maximum extinction of the SNAs' spectrum with each M^{2+} is drawn in a relative scale and compared in the inset.

Finally, we demonstrated that 'irreversible' assembly of SNAs could be also selectively induced by M^{2+}s. We took advantage of the permanent cleavage of DNA strands by highly reactive hydroxyl radical (HO·) that is catalytically generated by the DNA-bound M^{2+}s, particularly by Cu^{2+}, in the presence of H_2O_2.[51-53] The SNAs with shortened strands after the cleavage would partially lose their negative charges, leading to the destabilization and corresponding irreversible aggregation. The irreversible assemblies of the SNAs were prepared at various [Cu^{2+}]s (0.5 to 8 mM) in the presence of H_2O_2 (28 mM) for 1 hour, and the [Cu^{2+}]-dependent assembly properties were determined by UV-vis spectroscopy. As the concentration of Cu^{2+} increased, the spectroscopic data demonstrated that the SNAs assembled into larger NP clusters and eventually macroscopic aggregates (Figure 6a). This observation is apparently similar to that of the reversible assemblies (Figure 2a and Figure S3, †ESI). Importantly, however, the red-shifted UV-vis spectra were not recovered back to the initial one even after the addition of excess EDTA (see Figure S8, †ESI), evidently demonstrating irreversibility of these SNA assemblies. We further evaluated the capability of other M^{2+}s to irreversibly assemble SNAs under the same conditions ([M^{2+}] = 0.5 mM). Interestingly, Cu^{2+} exclusively induced the largest aggregate formation, while the others resulted in either negligible changes (Na^+ and Mg^{2+}), or only minor cluster formation of SNAs (Cd^{2+}, Mn^{2+}, Ni^{2+}, Zn^{2+}, and Co^{2+}). Although this result is rather based on the transition M^{2+}s' own catalytic properties regardless of their interactions with SNAs, it is still important to investigate how such properties affect the assembly properties of SNAs, especially considering the increasing interest in intracellular functions of SNAs as drug delivery materials or antisense reagents. In addition, while preliminary, this result also provides the possibility of their potential application to identify Cu^{2+}.

Conclusion

This work is the first demonstration of chemically controlled reversible assemblies of single-type SNAs without the assistance of any pre-designed DNA sequences and auxiliary organic chemicals, simply based on the fundamental interactions of the natural nucleobases and M^{2+}s, particularly Cu^{2+}. The investigation demonstrated in this work provides a milestone to be seriously considered as a new type of DNA bond for the growing interest in assembling nanomaterials into macroscopic structures, preventing undesirable non-specific binding of DNA-conjugated nanoprobes, and applying conventional nucleic acid chemistry to state-of-the-art nanotechnology.[54-59]

Acknowledgements

This work was supported by the Bio & Medical Technology Development Program of the NRF funded by the Korean government, MSIP (Grant No. 2015M3A9D7031015), Global PH.D Fellowship Program through the National Research Foundation of Korea funded by the Ministry of Education (grant# 2013H1A2A1032685) and Brain Korea 21 Plus Project in 2015. Korea Basic Science Institute (Seoul, Korea) is acknowledged for the ICP-MS measurement.

Experimental

Material and Methods

Gold(III) chloride trihydrate ($HAuCl_4 \cdot 3H_2O$, 99.9%, Cat. # 520918), sodium citrate tribasic dihydrate (99.9%, Cat. # S4641), L-ascorbic acid (99.9%, Cat. # A5960), TWEEN® 20 (Cat. # 9005-64-5), dithiothreitol (99.5%, Cat. # 43815), copper(II) chloride (99%, Cat. # 751944), zinc chloride 0.1 M solution (Cat. # 39059), cadmium(II) chloride (99.0%, Cat. # 20899), nickel(II) chloride (98%, Cat. # 339350), manganese(II) chloride (99%, Cat. # 244589), cobalt(II) chloride (98%, Cat. # 60818), magnesium(II) chloride (98%, Cat. # M8266), sodium chloride solution, (5 M, Cat. # S6546), hydrogen peroxide solution (30 % w/w, Cat. # H1009), and tris-EDTA buffer solution (100 mM, Cat. # T9285) were purchased from Sigma-Aldrich (St. Louis, MO, USA). The HPLC-purified monothiol DNA sequences (**S1**: 5′ HS-A_{10}-ATTATCACT 3′, **S2**: 5′ HS-A_{10}-AGTGATAAT 3′, **Dbl-S1**: 5′ ATTATCACT-ATTATCACT 3′, **Dbl-S2**: 5′ AGTGATAAT-AGTGATAAT 3′, **FS1**: 5′ ATTATCACT 3′, $\mathbf{A_{20}}$: 5′ HS-A_{20} 3′, $\mathbf{C_{20}}$: 5′ HS-C_{20} 3′, $\mathbf{T_{20}}$: 5′ HS-T_{20} 3′, and **3′ thiol-S1**: 5′ TCACTATTA-A_{20}-SH 3′) were purchased from GenoTech (Daejeon, Republic of Korea). The original **S1** and **S2** sequences contain only 9 nucleotides that participate in the hybridization, and do not form duplexes under the given experimental conditions (0.15 M NaCl, 25 °C). Therefore, we designed two new elongated complementary sequences (**Dbl-S1** and **Dbl-S2**), each of which is composed of two sequential repetitions of the original sequence, and thus, is two times as lengthy as the original one. The NAP-5 Sephadex® columns were purchased from GE Healthcare (Little Chalfont, UK). In all the experiments ultrapure water from a Direct-Q® 3 system (18.2 MΩ·cm, Millipore, Billerica, MA, USA) was used. Agilent 8453 UV-vis spectrophotometer (Agilent Technologies, Santa Clara, CA, USA) was used for UV-vis spectroscopic measurements.

Synthesis of Gold Nanoparticles

In a 100 mL Erlenmeyer flask, 49 mL of ultrapure water was heated to 100 °C. To the boiling water, 1 mL of a gold chloride ($HAuCl_4$) solution (12.7 mM) was injected, which was followed by an addition of 0.94 mL of a trisodium citrate solution (38.8 mM) with stirring. The color of the solution gradually turned red, indicative of the formation of gold nanoparticles. After 5 min, the gold nanoparticle solution was slowly cooled down to 25 °C with stirring and stored in the dark before use.

Synthesis of Spherical Nucleic Acids (SNAs)

The monothiol DNA sequences were deprotected by dithiothreitol (0.10 M in a 0.17 M phosphate buffer, pH 8.0), and purified by a NAP-5 column. The thiol DNA was combined with 1 mL of the gold nanoparticles (the final [DNA] ≈ 4.8 μM). This mixture solution was buffered at 0.15 M NaCl in a phosphate buffer (10 mM phosphate, pH 7.4, 0.01 % TWEEN® 20) and incubated for 12 h at 25 °C. To eliminate the unconjugated thiol DNA, the synthesized SNAs were centrifuged (13000 rpm, 20 min) to remove the supernatant, and redispersed in a desired buffer. This washing process was repeated 3 times.

Effect of M^{2+} on Dehybridization Properties of Duplex-Interconnected SNA Assemblies

To prepare the duplex-interconnected SNA assemblies, two complementary SNAs (**S1** and **S2**, each at 0.5 nM) were combined and allowed to hybridize at 25 °C for 12 h (0.15 M NaCl, 0.01 % TWEEN® 20). The final solution volume was 900 μL. After the completion of the hybridization, the SNA assembly solution was combined with 100 μL of an M^{2+} solution at a desired concentration. TWEEN® 20 plays an important role in preventing the SNAs from being adsorbed on the inner surface of the containers (plastic microtubes, glass vials, quartz cuvettes, etc.). The melting profiles of the SNA assemblies combined with an M^{2+} were obtained by monitoring the extinction change at 525 nm as the temperature increased from 25 to 75 °C at a rate of 1 °C/min using an Agilent 8453 UV-vis spectrophotometer.

M^{2+}-Mediated Reversible Assembly Formation of SNAs

The SNA assemblies were prepared using single type SNAs, not using two complementary SNAs. In a typical experiment, single type SNAs (900 μL) were combined with an M^{2+} solution (100 μL) at a desired concentration of M^{2+} (the final [SNA] = 1 nM). The mixture was kept at 25 °C for 12 h with stirring for the assembly formation. To reversibly disassemble the assembled SNAs, 10 μL of an EDTA solution (typically [EDTA] = final [M^{2+}]) was added to the 1 mL of the SNA assembly solution with vigorous stirring. The assembly properties of the SNAs were monitored by measuring their UV-vis spectrum using an Agilent 8453 UV-vis spectrophotometer.

ICP-MS Measurement

The single-type SNAs (**S1**, $\mathbf{A_{20}}$, $\mathbf{C_{20}}$, and $\mathbf{T_{20}}$) at 1 nM were combined with Cu^{2+} (1 μM for $\mathbf{A_{20}}$, $\mathbf{C_{20}}$, and $\mathbf{T_{20}}$; 0.5, 1, 2, 4, 6 μM for **S1**) for 3 h at 25 °C for the adsorption of Cu^{2+} to the SNAs. The final volume was 1 mL. The SNAs were centrifuged down (13000 rpm, 20 min), and the supernatant containing non-adsorbed free Cu^{2+} was collected and diluted 20 times for the ICP-MS measurement (Agilent 7700, Agilent Technologies). The final mole number of Cu^{2+} adsorbed to the SNAs was calculated by subtracting the mole number of the free Cu^{2+} from the initially given mole number of Cu^{2+}.

Irreversible Assembly Formation of SNAs

The SNAs (**S1**) were combined with Tween® 20 and H_2O_2 in an aqueous solution ([H_2O_2] = 28 mM, [SNA] = 1 nM, and 0.01% Tween® 20, as final concentrations), to which a Cu^{2+} stock solution at a desired concentration was spiked (final [Cu^{2+}] = 0 ~ 8 mM). The mixture was allowed to react for 1 h at 50 °C. The UV-vis spectra of the SNAs were obtained using an Agilent 8453 UV-vis spectrophotometer.

Notes and references

1. Spherical nucleic acids (SNAs) refer to spherical nanomaterials (e.g. spherical gold nanoparticles) densely conjugated with nucleic acids, or their coreless form after crosslinking of the nucleic acids at the base. More details of SNAs are introduced in Reference 2.
2. J. I. Cutler, E. Auyeung and C. A. Mirkin, J. Am. Chem. Soc., 2012, **134**, 1376-1391.
3. C. A. Mirkin, R. L. Letsinger, R. C. Mucic and J. J. Storhoff, Nature, 1996, **382**, 607-609.
4. N. L. Rosi and C. A. Mirkin, Chem. Rev., 2005, **105**, 1547-1562.
5. L. H. Tan, H. Xing and Y. Lu, Accounts Chem. Res., 2014, **47**, 1881-1890.
6. S. J. Barrow, A. M. Funston, X. Z. Wei and P. Mulvaney, Nano Today, 2013, **8**, 138-167.
7. K. Zhang, L. L. Hao, S. J. Hurst and C. A. Mirkin, J. Am. Chem. Soc., 2012, **134**, 16488-16491.
8. X. Zhang, M. R. Servos and J. W. Liu, J. Am. Chem. Soc., 2012, **134**, 7266-7269.

9. J.-S. Lee, J. J. Green, K. T. Love, J. Sunshine, R. Langer and D. G. Anderson, Nano Lett., 2009, **9**, 2402-2406.
10. R. Jin, G. Wu, Z. Li, C. A. Mirkin and G. C. Schatz, J. Am. Chem. Soc., 2003, **125**, 1643-1654.
11. L. H. Tan, H. Xing, H. Y. Chen and Y. Lu, J. Am. Chem. Soc., 2013, **135**, 17675-17678.
12. L. Di Michele, B. M. Mognetti, T. Yanagishima, P. Varilly, Z. Ruff, D. Frenkel and E. Eiser, J. Am. Chem. Soc., 2014, **136**, 6538-6541.
13. B. D. Smith and J. W. Liu, J. Am. Chem. Soc., 2010, **132**, 6300-6301.
14. J.-H. Oh and J.-S. Lee, Chem. Commun., 2010, **46**, 6382-6384.
15. S. M. Swasey, L. E. Leal, O. Lopez-Acevedo, J. Pavlovich and E. G. Gwinn, Sci. Rep., 2015, **5**, 10163.
16. A. B. Chinen, C. M. Guan and C. A. Mirkin, Angew. Chem.-Int. Edit., 2015, **54**, 527-531.
17. J. Poater, M. Swart, C. F. Guerra and F. M. Bickelhaupt, Chem. Commun., 2011, **47**, 7326-7328.
18. J. Poater, M. Swart, F. M. Bickelhaupt and C. F. Guerra, Org. Biomol. Chem., 2014, **12**, 4691–4700.
19. C. F. Guerra, T. v. d. Wijst, J. Poater, M. Swart and F. M. Bickelhaupt, Theor. Chem. Acc., 2010, **125**, 245-252.
20. S. Nakano, M. Fujimoto, H. Hara and N. Sugimoto, Nucleic Acids Res., 1999, **27**, 2957-2965.
21. X. Xue, F. Wang and X. Liu, J. Am. Chem. Soc., 2008, **130**, 3244-3245.
22. J. Du, L. Jiang, Q. Shao, X. Liu, R. S. Marks, J. Ma and X. Chen, Small, 2013, **9**, 1467-1481.
23. B. Sepulveda, P. C. Angelome, L. M. Lechuga and L. M. Liz-Marzan, Nano Today, 2009, **4**, 244-251.
24. S. K. Ghosh and T. Pal, Chem. Rev., 2007, **107**, 4797-4862.
25. G. L. Eichhorn and Y. A. Shin, J. Am. Chem. Soc., 1968, **90**, 7323-7328.
26. V. A. Bloomfield, Biopolymers, 1991, **31**, 1471-1481.
27. V. A. Bloomfield, Biopolymers, 1997, **44**, 269-282.
28. R. J. P. Williams, Calcium Chemistry And Its Relation To Protein Binding, North-Holland, New York, 1977.
29. R. M. Izatt, Christen.Jj and J. H. Rytting, Chem. Rev., 1971, **71**, 439-481.
30. J. G. Duguid and V. A. Bloomfield, Biophys. J., 1995, **69**, 2642-2648.
31. G. L. Eichhorn, P. Clark and E. D. Becker, Biochemistry, 1966, **5**, 245-253.
32. R. K. O. Sigel and H. Sigel, Accounts Chem. Res., 2010, **43**, 974-984.
33. H. Pezzano and F. Podo, Chem. Rev., 1980, **80**, 365-401.
34. B. H. Geierstanger, T. F. Kagawa, S. L. Chen, G. J. Quigley and P. S. Ho, J. Biol. Chem., 1991, **266**, 20185-20191.
35. P. M. Cullis, J. D. McClymont, M. N. O. Bartlett and M. C. R. Symons, J. Chem. Soc. Chem. Comm., 1987, 1859-1861.
36. M. Palaniandavar, I. Somasundaram, M. Lakshminarayanan and H. Manohar, J. Chem. Soc. Dalton., 1996, 1333-1340.
37. A. Kundagrami and M. Muthukumar, J. Chem. Phys., 2008, **128**, 244901.
38. S. Kewalramani, J. W. Zwanikken, R. J. Macfarlane, C.-Y. Leung, M. O. de la Cruz, C. A. Mirkin and M. J. Bedzyk, ACS Nano, 2013, **7**, 11301-11309.
39. E. Allahyarov, H. Lowen and G. Gompper, Phys. Rev. E, 2003, **68**, 061903.
40. H. Sigel, Chem. Soc. Rev., 1993, **22**, 255-267.
41. C. Zimmer, G. Luck, Fritzsch.H and H. Triebel, Biopolymers, 1971, **10**, 441-463.
42. L. Rulisek and J. Sponer, J. Phys. Chem. B, 2003, **107**, 1913-1923.
43. M. Noguera, J. Bertran and M. Sodupe, J. Phys. Chem. A, 2004, **108**, 333-341.
44. M. Noguera, J. Bertran and M. Sodupe, J. Phys. Chem. B, 2008, **112**, 4817-4825.
45. J. H. Oh and J.-S. Lee, Anal. Chem., 2011, **83**, 7364-7370.
46. W. Forster, E. Bauer, H. Schutz, H. Berg, N. M. Akimenko, L. E. Minchenkova, Y. M. Evdokimov and Y. M. Varshavsky, Biopolymers, 1979, **18**, 625-661.
47. E. V. Hacki and Y. P. Blagoi, Biopolymers, 2005, **77**, 315-324.
48. A. Kratz, M. Ferraro, P. M. Sluss and K. B. Lewandrowski, New Engl J Med, 2004, **351**, 1548-1563.
49. S. L. Tompsett, Biochem. J., 1934, **28**, 1544-1549.
50. S. L. Tompsett and D. F. Anderson, Brit. J. Exp. Pathol., 1935, **16**, 67-69.
51. M. Dizdaroglu, G. Rao, B. Halliwell and E. Gajewski, Arch. Biochem. Biophys., 1991, **285**, 317-324.
52. O. I. Aruoma, B. Halliwell, E. Gajewski and M. Dizdaroglu, Biochem. J., 1991, **273**, 601-604.
53. A. Mendez-Garrido, M. Hernandez-Rodriguez, R. Zamorano-Ulloa, J. Correa-Basurto, J. Elena Mendieta-Wejebe, D. Ramirez-Rosales and M. Cecilia Rosales-Hernandez, Neurochem. Res., 2014, **39**, 2093-2104.
54. M. R. Jones, N. C. Seeman and C. A. Mirkin, Science, 2015, **347**, 1260901.
55. T. Ihara, H. Ohura, C. Shirahama, T. Furuzono, H. Shimada, H. Matsuura and Y. Kitamura, Nat. Commun., 2015, **6**, 6640.
56. H. Liang, X. B. Zhang, Y. F. Lv, L. Gong, R. W. Wang, X. Y. Zhu, R. H. Yang and W. H. Tan, Accounts Chem. Res., 2014, **47**, 1891-1901.
57. A. V. Pinheiro, D. Han, W. M. Shih and H. Yan, Nat. Nanotechnol., 2011, **6**, 763-772.
58. N. C. Seeman, Nature, 2003, **421**, 427-431.
59. J.-J. Xu, W.-W. Zhao, S. Song, C. Fan and H.-Y. Chen, Chem. Soc. Rev., 2014, **43**, 1601-1611.